

Photochemical Pre-Treatment to Quantify Iron in Thin Films

Rafael L. Germscheidt,^a Cleiber C. Morais,^a Danielle S. Francischini,^a
Marco Aurélio Z. Arruda^a and Juliano A. Bonacin[✉]*,^a

^aInstituto de Química, Universidade Estadual de Campinas, 13083-970 Campinas-SP, Brazil

Metal-based catalysts are indispensable in modern chemistry and one of the biggest challenges for industrial applications is to quantify their performance and stability. The metrics of performance can be obtained in terms of the turnover number and turnover frequency, and the stability might be associated with the leaching of the heterogeneous catalysts. Thus, metal quantification is the starting point to understand and evaluate the features of catalysts. Among the technologies for metal determination, spectrophotometric analysis stands out for being cheap and easy to perform. However, the challenge is the sample preparation to direct quantification from the heterogeneous materials. Herein, it is shown how important is the photochemical pre-treatment for the quantification of the total iron from heterogeneous thin films composed of iron-based materials. The photochemical approach was used to ensure a full dissociation of iron ions before the quantification. This method was revealed to be highly effective and precise, having a wide range of applications for different iron-based catalysts.

Keywords: iron quantification, photochemical pre-treatment, photolabilization, iron-based catalyst, thin films

Introduction

The deposition of catalysts thin films on electrode surfaces is essential for heterogeneous electrocatalysis reactions. The evaluation of the metal content, numbers of active sites besides the level of conversion are extremely necessary to determine the efficiency, activity, and stability of a specific catalyst.^{1,2} Parameters such as turnover number (TON), turnover frequency (TOF), and long-term stability depend on the quantification of active sites on the catalysts.^{3,4}

Iron-based catalysts are widely used in the chemical industry. Furthermore, these catalysts produce outstanding activities and efficiencies in the water splitting process where the water is converted into green hydrogen.^{1,5-8} The activity and efficiency of the catalyst are directly related to the number of active sites, and it is usually linked to metal sites, as they facilitate electron transfer reactions and are the main responsible for the catalyst efficiency.⁹⁻¹² Thus, an accurate iron quantification is essential to evaluate an iron-based catalyst.

The determination of metal ions can be performed by several analytical techniques, such as atomic absorption

spectroscopy (AAS), inductively coupled plasma optical emission spectrometry (ICP OES), inductively coupled plasma mass spectrometry (ICP-MS),^{13,14} and spectrophotometry (UV-Vis).¹⁵ Among these techniques, spectrophotometry stands out for being simple, efficient, fast, and presenting low cost for both sample preparation and equipment maintenance. Besides, its spectra are very simple to be interpreted.¹⁶⁻¹⁹ The spectrophotometric determination in the UV-Vis region generally requires the use of other compounds to trigger some changes in the species of interest (analytes), in order to increase the analytical sensitivity and selectivity.^{15,19}

Given this scenario, the biggest challenge to calculate the amount of iron in these catalysts is the fact that most of them are based on complexed structures and/or molecules, where the iron atoms are complexed with different ligands. Therefore, an additional sample preparation step is required before performing spectrophotometric analysis. This is an important step, and it is responsible for providing a dissociation of the iron ion from its ligands and allowing its coordination with the compound responsible for increasing the analytical sensitivity and selectivity, typically 1,10-phenanthroline (phen) for iron quantification.

There are different methods presented in the literature for sample preparation for elemental analysis, including the

*e-mail: jbonacin@unicamp.br

Editor handled this article: Célia M. Ronconi (Associate)

use of ultrasonic waves, acid digestion, high temperature hydrolysis, microwave radiation degradation, the use of organic solvents, combustion and finally photochemical methods using UV light.²⁰⁻²³ The use of photolysis, a photochemical process that uses light (UV or visible)²⁴ stands out as a fast, cheap and environmentally friendly method, using only energy source and no side solvent or heating source to easily promote the complex dissociation by labializing the main ligands.^{21,25} Hence, photolysis has been widely applied in the last years to dissociate Fe ions from complex structures and/or molecules, allowing an effective labialization of different ligands, such as cyanide (CN), oxides, organic ligands, chloride (Cl⁻) and so on.^{21,25-29}

Therefore, herein we present a photolabilization strategy of iron to allow precise quantification of this metal from some iron-based catalysts, such as Prussian Blue, cobalt-iron Prussian Blue analog, hematite, nickel-iron oxyhydroxide, and cobalt-iron oxide.

Experimental

Preparation of the catalyst

All reagents were obtained from Sigma-Aldrich (São Paulo, Brazil).

Before catalyst film deposition, fluorine-doped tin oxide (FTO) glass substrates of 1 × 2.5 cm² were cleaned using isopropyl alcohol in an ultrasonic bath for 10 min, rinsed with distilled water, and cleaned again in an ultrasonic bath using distilled water for 10 min. After that, the substrates were annealed in a muffle at 400 °C for 30 min.¹²

Hematite (Fe₂O₃)

Hematite films were obtained by immersing the electrode in a solution containing 0.1 mol L⁻¹ of FeSO₄, 0.1 mol L⁻¹ of FeCl₃. Then, metallic iron was reduced over the electrode surface by applying a constant potential of -1.1 V × saturated calomel electrode (SCE) for 300 s. The electrode was dried and then, the film was submitted to thermal treatment in a muffle at 400 °C for 150 min.

Bimetallic hydroxide (NiFe(oxy)OH)

Bimetallic hydroxide films were obtained according to the method previously reported by our group.³⁰ Since the goal of this work was only the iron quantification in the catalyst, following the methodology, we also used 3D printed electrodes for the deposition of NiFeOOH catalyst. The electrode activation process was also followed before the catalyst deposition. Then, the electrode was immersed in

a solution containing 90% of NiSO₄ and 10% of FeSO₄ with the total metal content of 10 mol L⁻¹. Electrodeposition was carried out by chronopotentiometry as previously reported, by applying a cathodic current density of 50 μA cm⁻² for 1125 s.

Prussian Blue (PB)

PB films were obtained by immersing the electrode in a solution containing 1 mmol L⁻¹ of [Fe(CN)₆]³⁻, 1 mmol L⁻¹ of FeCl₃, 0.1 mol L⁻¹ of KNO₃, and 0.1 mol L⁻¹ of HCl. Then, 10 cycles were performed from 0.37 to 0.8 V × SCE, on a scan rate of 8 mV s⁻¹. After this, a blue film was observed on the electrode.

CoFe Prussian Blue analogues (CoFePBA)

CoFePBA films were obtained as reported. Cobalt(II) chloride (12 mmol) was dissolved in 80 mL of Milli-Q water to form a solution A. Potassium hexacyanoferrate(III) (8 mmol) was dissolved in 80 mL of Milli-Q water to form a solution B. Then, solution A was added into solution B under magnetic stirring for 1 h. After continuous stirring for 2 h, the homogeneous solution was maintained at a low temperature for 12 h. The precipitate was collected by centrifugation and exhaustively washed with Milli-Q water to ensure the removal of any trace of precursors and after this, the solid was dried at 60 °C overnight. The films were prepared by a drop-casting method. The ink of catalyst was prepared by a mixture of the solid compounds (5 mg), Milli-Q water (100 μL), dimethylformamide (DMF) (200 μL), and Nafion[®] (20 μL). Then, the mixture was sonicated for 30 min to obtain a homogeneous ink and 25 μL of the ink was dropped into an FTO electrode to cover a 1 cm² area. The electrodes were dried at a vacuum system to remove the solvent.

CoFe oxide (CoFeO_x)

CoFe oxide was obtained from the CoFePBA framework. So, the modified electrode was submitted to thermal treatment in a muffle at 400 °C for 150 min.

Preparation for iron quantification

Prior to the iron determination methodology, the oxide films were dissolved with 5 mL of a 0.1 mol L⁻¹ hydrofluoric acid (HF) solution, and the PB films dissolved with 5 mL of a 0.1 mol L⁻¹ sodium hydroxide (NaOH) solution, in an ultrasonic bath, to assure complete removal of the film. The obtained solutions were transferred to 25 mL volumetric

flasks. These final solutions were then used for the Fe determination analysis.

Electronic spectroscopy

Spectra of aqueous solutions in the UV-Vis region were obtained using a Bel Photonics UV-M51 UV-visible absorption spectrophotometer (Monza, Italy), with a 1 cm quartz cuvette, in the region from 200 to 600 nm.

Results and Discussion

Fe concentration calibration

The use of phen to quantify Fe^{2+} ions is a well-known method since this bidentate chelating agent has two nitrogen atoms at the *ortho* positions of the rigid half-ring structure, which can coordinate with Fe^{2+} ions, forming a complex,¹⁵ as it can be seen in Figure 1a. This molecule is known as a π -acceptor ligand and its coordination with Fe^{2+} produces a specific color in the visible region (orange-red color) assigned, as mentioned before, to metal-to-ligand charge transferences ($\text{Fe}(d) \rightarrow \text{phen}(\pi^*)$). In the $[\text{Fe}(\text{phen})_3]^{2+}$ complex, the metal d-orbitals will give rise to the highest occupied molecular orbitals (HOMO), while the p-orbitals from the carbon and nitrogen in the phen, will give rise to the lowest unoccupied molecular orbitals (LUMO), Figure 1a. The absorption band on the UV-Vis electronic spectrum of $[\text{Fe}(\text{phen})_3]^{2+}$ (Figure 1b) in a smaller wavelength, 267 nm, can be assigned to the intraligand $\pi \rightarrow \pi^*$ transitions for phen. Furthermore, the adsorption bands identified in higher wavelengths, 475 and 510 nm, can be assigned to the metal to ligand charge transference (MLCT) $\text{Fe}(d) \rightarrow \text{phen}(\pi^*)$ transitions. The maximum absorbance for the MLCT transition is found

around 510 nm and its intensity is directly proportional to the $[\text{Fe}(\text{phen})_3]^{2+}$ complex concentration in the solution.^{31,32}

The $[\text{Fe}(\text{phen})_3]^{2+}$ complex is produced immediately in the presence of Fe^{2+} ions and phen in an aqueous solution and it can be easily detected by UV-Vis spectroscopy. However, its formation does not occur instantly if the iron ions are already complexed with other ligands, which is the case for some iron-based catalysts, such as PB, hematite, or some iron oxyhydroxide. Thereby, it is not possible to use this methodology directly to quantify the amount of iron in these samples due to their low dissociation kinetics and solubility product constant.

PB, for example, is a kind of coordination compound formed by the mixture of Fe^{3+} and $[\text{Fe}(\text{CN})_6]^{4-}$ and its structure and analogues are widely studied to be used as catalysts.³³ In this case, Fe^{3+} ions coordinate with N of the cyanide group to produce a 3D framework. The called "insoluble Prussian Blue" ($\text{Fe}_4[\text{Fe}(\text{CN})_6]_3 \cdot n\text{H}_2\text{O}$) is a very stable blue solid, and it has the value of $K_{\text{ps}} = 3 \times 10^{-41}$.³⁴ Considering the evaluation of the iron content in a PB film, the first step to analyze this metal content in a thin film is to solubilize the material. This step can be easily done in this case with an alkaline solution. During the solubilization, Fe^{3+} (can produce a hydroxy/oxo) and $[\text{Fe}(\text{CN})_6]^{4-}$ are formed. Thus, it is necessary to replace the cyanide ligand by phen.

Studies^{21,25} show that although these aqueous complexes dissociate slowly in the darkness, upon exposure to UV light they can dissociate easily, releasing cyanide. Given this motivation, $[\text{Fe}(\text{CN})_6]^{4-}$ solutions were initially used to obtain a pattern for the iron concentration when complexed with phenanthroline, acquiring a calibration curve in different concentrations, from 1.2×10^{-6} to $7.1 \times 10^{-4} \text{ mol L}^{-1}$, as seen in Figure 2. The solutions were

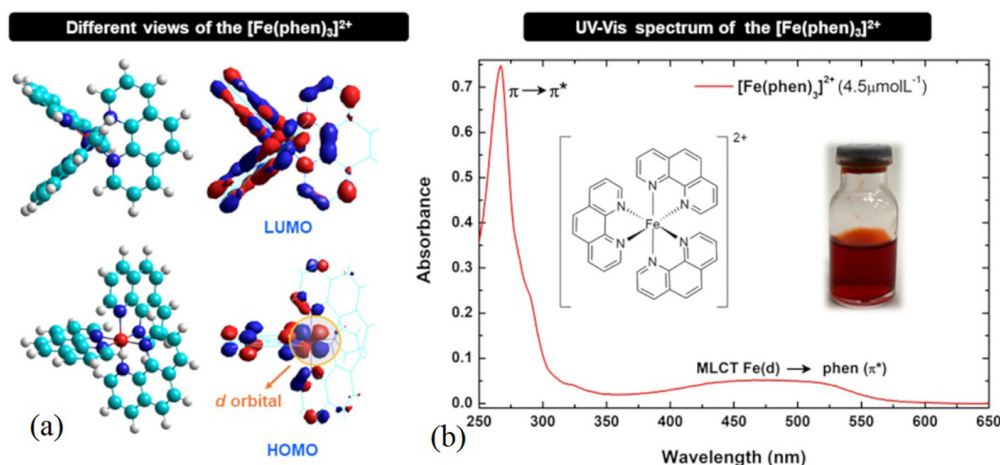


Figure 1. (a) Structure of the $[\text{Fe}(\text{phen})_3]^{2+}$ complex and its frontier orbitals; (b) UV-Vis electronic spectrum of $[\text{Fe}(\text{phen})_3]^{2+}$ (concentration: $4.5 \mu\text{mol L}^{-1}$) and picture of a concentrated solution of the complex.

submitted to UV-A light incidence for 1 h, in a photoreactor (Figure S1, Supplementary Information (SI) section). This light provides the necessary energy for the complex dissociation to happen and consequently the complexation with phenanthroline present in the solution. After 1 h, it was possible to observe a change in the color, with an orange-red color appearance (Figure S2, SI section), with a color intensity related to the sample concentration, as can be seen in Figure 2a. Besides, it was also possible to identify the band related to the $[\text{Fe}(\text{phen})_3]^{2+}$ complex in the UV-Vis spectrum at 510 nm (Figure 2b).

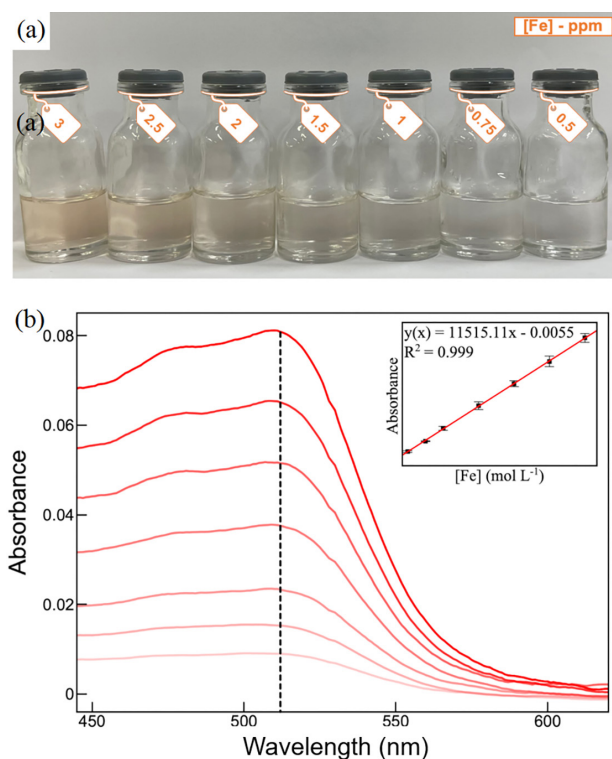


Figure 2. (a) Solutions of $[\text{Fe}(\text{CN})_6]^{4-}$ in different concentrations after the exposure to UV light; (b) calibration curve for $[\text{Fe}(\text{CN})_6]^{4-}$ with phenanthroline and UV-light incitation. Insert indicates the obtained calibration curve with an error bar obtained from $n = 3$.

The comparison among the UV-A light wavelength, the intensity and the $[\text{Fe}(\text{CN})_6]^{4-}$ UV-Vis spectrum (Figure S3, SI section) allows a discussion about the mechanism of the reaction. As it can be seen, the $[\text{Fe}(\text{CN})_6]^{4-}$ spectrum has a characteristic band at 330 nm, which can be assigned to the ${}^2T_{2g} \rightarrow {}^2A_{1g}$ transition.^{35,36} The UV-light wavelength ranges from 297 to 422 nm, and the part that overlaps with the $[\text{Fe}(\text{CN})_6]^{4-}$ absorption band is around 297–365 nm. This shows a direct overlap between the UV-light absorption bands and the band interactions between iron and cyanide. Based on this, two different possible UV-light-dependent mechanisms were suggested in Figure S4 (SI section), and both of them can happen and contribute to the formation of

the $[\text{Fe}(\text{phen})_3]^{2+}$ complex. In the first proposal, the UV-light exposure contributes to the dissociation of $[\text{Fe}(\text{CN})_6]^{4-}$, which results in the formation of $[\text{Fe}(\text{OH})_2]^{4+}$. Then, this complex, in the presence of phenanthroline and by a substitution mechanism, changes the ligands and forms the complex of interest, $[\text{Fe}(\text{phen})_3]^{2+}$. The other possibility is the dissociation by the UV-light exposure with a direct complexation of iron and phenanthroline, without the need for the intermediate aquo complex.

After the complex formation by the UV-light exposure, the band was identified on the UV-Vis spectrum, and this band absorbance intensity was related to the Fe concentration, allowing the obtention of a linear calibration curve, with an R^2 (coefficient of determination) = 0.999 (Figure 2).

To obtain a more accurate result on the iron quantification, which is an extremely important factor for the TON or TOF calculation, for example, the calibration curve was obtained 3 different times, using different solutions. The results were similar, and the amount of iron was calculated using an average of the 3 analyses:

$$y(x) = 11515x - 0.0055 \quad (1)$$

The calibration curve was validated and tested with spiked iron sample, and through the limit of detection (LOD) and limit of quantification (LOQ), and more details can be seen in the SI section. The obtained results for LOD and LOQ were 1.3132×10^{-7} and 3.8163×10^{-7} , respectively, which are smaller than the calibration curve first point (1.18402×10^{-6}), thus, the obtained calibration curve is accurate for these concentrations. As it can be seen in Table S1 and Figure S5 (SI section), for the spiked samples, satisfactory recovery values of 97.56 and 96.10% were obtained for both evaluated samples, indicating an effective determination of Fe without significant matrix effects. Furthermore, the accuracy was checked by comparing the quantification of iron also with ICP-MS analysis. The results can be seen in Figure S6 and Table S3 (SI section), and they indicate an accurate determination of Fe with the proposed technique, validating the method with ICP-MS recoveries ranging from 90 to 120%.

Iron quantification in different catalysts

After the calibration curve preparation and testing with FeCl_3 and $[\text{Fe}(\text{CN})_6]^{4-}$ + UV-A light, the method was applied for the iron determination in a PB catalyst. The PB film was prepared and dissolved with NaOH into a solution to be analyzed, according to the details provided in the Experimental section.

The study for the determination of the total iron amount was carried out in 4 different conditions. Firstly, the catalyst solutions were analyzed only with the addition of phen, which can indicate the amount of free Fe^{2+} at the beginning of the reaction (5 min + phen). Then, an excess of a reducing agent (hydroxylammonium chloride, $\text{NH}_2\text{OH}\cdot\text{HCl}$) was added to the solution to make sure that all free iron was converted into Fe^{2+} (5 min + phen + $\text{NH}_2\text{OH}\cdot\text{HCl}$). Furthermore, the second solution (5 min + phen + $\text{NH}_2\text{OH}\cdot\text{HCl}$) was split into two others. One of them was kept in the dark for 1 h (1 h, dark, phen + $\text{NH}_2\text{OH}\cdot\text{HCl}$) and the other was added into the UV reactor for UV-light exposure (1 h, UV, phen + $\text{NH}_2\text{OH}\cdot\text{HCl}$). In this way, we were able to evaluate the UV-light exposure effect. The results can be seen in Figure 3, Tables 1 and 2.

The PB structure was shown to be very stable, and its initial analysis showed an amount of iron of 17.15 ± 1.60 and 21.54 ± 1.06 nmol for only phenanthroline addition and after the addition of $\text{NH}_2\text{OH}\cdot\text{HCl}$, respectively. This small amount of Fe^{2+} free, in the beginning, proves the need for an external energy source to help with the Fe^{2+} dissociation.

After 1 h, it was possible to observe an increase in the iron amount, 51.45 ± 0.33 and 145.5 ± 4.0 nmol, for dark and UV-light exposure, respectively. The results are presented in Table 1.

The $[\text{Fe}(\text{phen})_3]^{2+}$ formation mechanism would be the same as the one proposed for $[\text{Fe}(\text{CN})_6]^{4-}$ (Figure S4, SI section). Thus, this method can be suitable to quantify iron in the PB structure, as long the solution is exposed to UV-light for 1 h before the analysis. This approach ensures the total dissociation of iron from cyanide, allowing the obtention of precise iron quantification. This final iron amount, in nmol, could be further used to calculate TOF (equations 2 and 3) and evaluate the activity and efficiency of the catalyst, for example.

$$\text{TON} = \text{mols oxygen/mols catalyst} \quad (2)$$

$$\text{TOF} = \text{TON/time (s)} \quad (3)$$

Since the quantification method was shown to be highly effective for PB thin films, the same method was applied

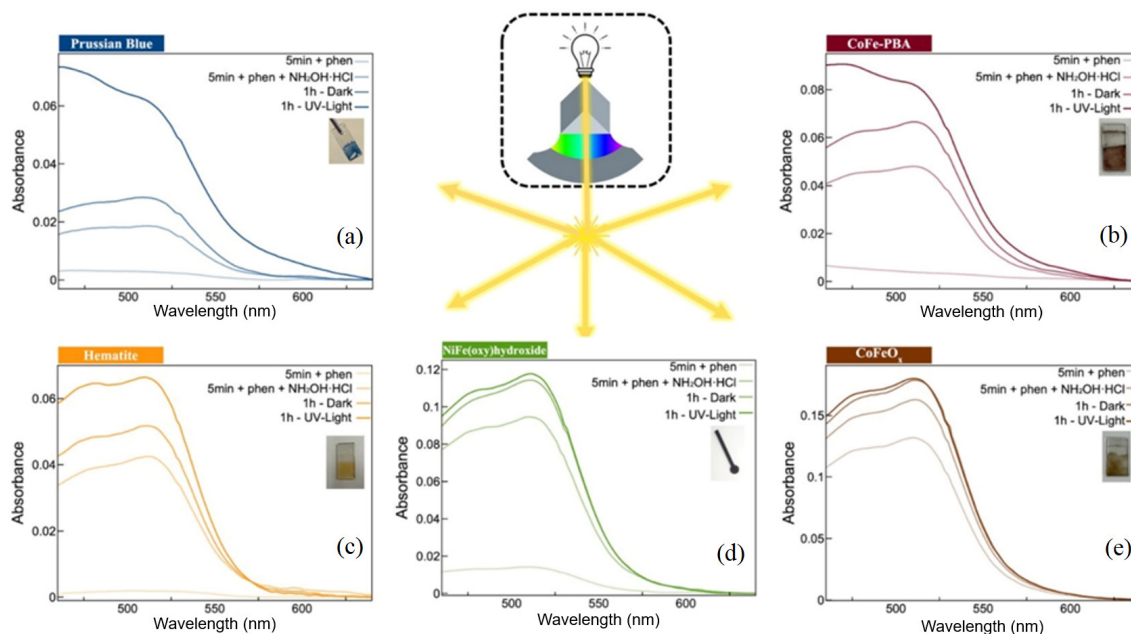


Figure 3. UV-Vis electronic spectrum for iron determination on catalysts. (a) Prussian Blue; (b) Co-Fe Prussian Blue analogue (CoFe-PBA); (c) hematite (Fe_2O_3); (d) Ni-Fe (oxy)hydroxide (NiFe_xOOH); (e) Co-Fe oxide (CoFeO_x) in different conditions.

Table 1. Iron concentration for each catalyst in different conditions of analysis ($n = 3$)

Condition	Iron concentration / nmol				
	Prussian Blue	CoFePBA	Fe_2O_3	NiFe(oxy)OH	CoFeO_x
5 min, without $\text{NH}_2\text{OH}\cdot\text{HCl}$	17.15 ± 1.60	6.180 ± 0.040	14.33 ± 0.45	41.48 ± 1.21	297.2 ± 1.1
5 min, with $\text{NH}_2\text{OH}\cdot\text{HCl}$	21.54 ± 1.06	36.82 ± 0.05	104.2 ± 0.8	215.6 ± 0.5	364.1 ± 0.5
1 h, dark	51.45 ± 0.33	155.5 ± 0.1	124.2 ± 3.2	260.7 ± 0.1	398.0 ± 3.2
1 h, UV-light	145.5 ± 4.0	190.8 ± 0.9	157.2 ± 1.9	266.4 ± 0.7	400.6 ± 0.5

for the study and quantification of a PB analog prepared with cobalt and iron. CoFe-PBA is an analog to the PB, in which Fe^{3+} can be substituted by Co^{2+} , being represented by $\text{Co}_3[\text{Fe}(\text{CN})_6]_2 \cdot n\text{H}_2\text{O}$. These Co-PBA stand out for their great activity towards the oxygen evolution reaction since their high conductivity gives rise to exposure of more active sites and facilitates the electron transfer during oxygen evolution reaction.^{12,37,38} Its structure was also shown to be very stable in the beginning, and its initial analysis showed an amount of iron of 6.180 ± 0.040 and 36.82 ± 0.05 nmol for only phenanthroline addition and after the addition of $\text{NH}_2\text{OH} \cdot \text{HCl}$, respectively.

This indicates that a low content of iron was available at the beginning of the reaction to be coordinated with phen. This small amount of iron available in the beginning indicates a similar behavior to PB and the need for UV-light exposure to allow iron dissociation. After 1 h, it is possible to observe an increase in the iron amount, 155.5 ± 0.1 and 190.8 ± 0.9 nmol, for dark and UV-light exposure, respectively. These results indicate that UV-light exposure contributes to the total dissociation of iron from cyanide. The $[\text{Fe}(\text{phen})_3]^{2+}$ complex formation mechanism would be the same as the one proposed for $[\text{Fe}(\text{CN})_6]^{4-}$ (Figure S4), and both proposals, with and without the formation of the aquo intermediate would be possible. Moreover, as it can be seen in Figure S7, SI section, the cobalt-phenanthroline complex has absorption bands around 200 and 294 nm, and it does not present any band close to 510 nm, therefore, even if the compound Co-phen is formed, it does not interfere with the iron quantification. Thus, this method can also be considered suitable for iron quantification on PBAs thin films, with precise and accurate results, see Table 1 and Figure 3.

Considering the obtained results for PB and PBA, the method was also applied for iron quantification in other iron-based catalyst's thin films, such as hematite (Fe_2O_3), bimetallic Ni-Fe oxyhydroxide (NiFeOOH), and a bimetallic CoFe oxide (CoFeOx), and the film preparation details can be found in the Experimental section.

Hematite (Figure 3c) has a rhombohedral structure, consisting of an intense structure connected to the Fe^{3+} cation in octahedral coordination with oxygen in the hexagonal closed packing system, and it is widely used as a catalyst.^{39,40} The predominance of Fe^{3+} in the structure was proven by the first analysis, by only adding phenanthroline, in which the amount of iron present was 14.33 ± 0.45 nmol, and after the addition of $\text{NH}_2\text{OH} \cdot \text{HCl}$, the iron amount increased to 104.2 ± 0.8 nmol. After 1 h, it is possible to observe an increase in the iron amount, 124.2 ± 3.2 and 157.2 ± 1.9 nmol, for dark and UV-light exposure, respectively. In Table 1 is possible to see all results.

This result indicates that the UV-light exposure ensures the total amount of iron quantification, assuring that every iron atom is free to be coordinated with phenanthroline. However, the absence of UV-light (dark) also allowed a high amount of free iron after 1 h (Table 1). Two pathways could be proposed to happen during the metal labilization and coordination of Fe^{2+} with phen. One is based on UV-light labilization and the other takes place in the dark (Figure S8, SI section). The mechanisms were proposed according to the association between the UV-light reactor wavelength intensity and the Fe_2O_3 absorption spectrum (Figure S9, SI section). As it can be seen, the hematite spectrum has characteristics bands at 270, 294, and 333 nm. These bands can be assigned to the ligand-to-metal charge-transfer transitions and partly from the contributions of the Fe^{3+} ligand field transition ${}^6\text{A}_1 \rightarrow {}^4\text{T}_1$ (${}^4\text{P}$), ${}^6\text{A}_1 \rightarrow {}^4\text{E}$ (${}^4\text{D}$), and ${}^6\text{A}_1 \rightarrow {}^4\text{T}_2$ (${}^4\text{D}$).^{41,42} The UV light reactor wavelength ranges from 297 to 422 nm, and the part that overlaps with the hematite absorption bands is around 297-365 nm, comprising UV wavelengths, having a direct effect on the band interactions between iron and oxygen.

Based on that, for the time-dependent mechanism, it is believed that in solution, the iron oxide forms FeOOH , and in the presence of acid (H^+), it can form $\text{Fe}(\text{OH})_2^+$; then, by a ligand substitution reaction, in the presence of phenanthroline, can form the color complex $[\text{Fe}(\text{phen})_3]^{2+}$. Thus, this method is also observed as a suitable method for iron quantification in hematite films, presenting promising results. Furthermore, even though UV-light exposure does not have a greater effect on the iron dissociation, it is still necessary to ensure a total quantification of iron, as it can be seen in Table 1.

Ni(oxy)hydroxides (Figure 3d) were also studied since they are well-known structures with a wide application as catalysts, especially for the water oxidation reaction. Also, its activity had been shown to increase when doped with other first-row transition metals, particularly iron. And since the catalyst activity is directly related to the amount of iron that is present in the structure, iron quantification in these catalysts is essential.^{30,43} The predominance of Fe^{3+} was also found in this structure, since by only adding phenanthroline the amount of iron present was 41.48 ± 1.21 nmol, and after the addition of $\text{NH}_2\text{OH} \cdot \text{HCl}$, the iron amount increased to 215.6 ± 0.5 nmol. After 1 h, it is possible to observe an increase in the iron amount, 260.7 ± 0.1 and 266.4 ± 0.7 nmol, for dark and UV-light exposure, respectively. The results indicate that the UV-light effect in the dissociation of iron is almost neglectable, being responsible for only 2.22% of the total amount of iron (Table 2). The $[\text{Fe}(\text{phen})_3]^{2+}$ complex formation mechanism would be the same as the one proposed for hematite (Figure S8), mainly following

Table 2. Free Fe²⁺ percentage in each condition, assuming the last analysis as 100% of free iron

Condition	Free Fe ²⁺ / %				
	Prussian Blue	CoFePBA	Fe ₂ O ₃	NiFe(oxy)OH	CoFeO _x
5 min, without NH ₂ OH.HCl	11.79	3.24	9.19	15.57	74.20
5 min, without NH ₂ OH.HCl	14.81	19.29	66.29	80.93	90.88
1 h, dark	35.37	81.46	78.99	97.88	99.35
1 h, UV-light	100.0	100.0	100.0	100.0	100.0

the time-dependent mechanism, which is responsible for the formation of 97.88% of the [Fe(phen)₃]²⁺ complex. This may be related to a different and weaker bond between iron and oxygen, due to the presence of another metal (Ni), a different atom with a higher electronegativity in the structure, contributing to an easier and faster dissociation. This easier dissociation may be related to the fact that since Ni has a higher electronegativity, this would concentrate the electronic density around Ni and the bond between oxygen and Fe would become weaker, therefore, facilitating the labilization of the iron-oxygen bond; thus, making the UV-light exposure almost irrelevant. Besides, according to the literature, the coordination of phenanthroline to nickel atoms has an absorption band around 292 nm,⁴⁴ and it does not present any band close to 510 nm, therefore, even if some phenanthroline that is present in the solution is being coordinated to Ni, it does not interfere with the iron quantification. Therefore, the method of iron quantification with phenanthroline can also be applied for some iron-based (oxy)hydroxides, even without the need for UV-light exposure.

CoFeO_x (Figure 3e) was also studied since it has been extensively used as a catalyst for both electrochemical and photoelectrochemical water splitting, being able to achieve outstanding results. Also, the understanding of iron amount can help understand the catalyst activity.⁴⁵ The results indicate that CoFeO_x has a predominance of Fe²⁺ on its structure, since by only adding phenanthroline the amount of iron present was 297.2 ± 1.1 nmol, and after the addition of NH₂OH·HCl, the iron amount increased to 364.1 ± 0.5 nmol. After 1 h, it is possible to observe an increase in the iron amount, 398.0 ± 3.2 and 400.6 ± 0.5 nmol, for dark and UV-light exposure, respectively. The results indicate that the UV-light effect in the dissociation of iron is almost neglectable, since the small difference in the amount of iron in the dark and with UV-light exposure, around 2.6 nmol, is covered by the standard deviation. The [Fe(phen)₃]²⁺ complex formation mechanism would be the same as the one proposed for hematite (Figure S8), only following the time-dependent mechanism, which is responsible for the total dissociation of iron atoms and formation of the [Fe(phen)₃]²⁺ complex. Thus, it is possible to conclude that a mix of metals, specially when using metals with higher electronegativity, changes

the stability of Fe–O bonds, making the dissociation easier, which makes the use of UV-light unnecessary. Besides, as it was aforementioned and can be seen in Figure S7, the cobalt-phenanthroline complex has absorption bands around 200 and 294 nm, and it does not present any band close to 510 nm, therefore, even if some phenanthroline is present in the solution coordinated to Co, it does not interfere with the iron quantification. Therefore, the method of iron quantification with phenanthroline can also be applied for some iron-cobalt-based (oxy)hydroxides, presenting great results, even without the need for UV-light exposure.

All obtained results can be found in Table 1 and the percentage of iron in each analysis is summarized in Table 2.

Table 2 presents a comparison of the percentage of available Fe²⁺ in each of the four conditions, assuming the last (1 h, UV-light) provides a total iron dissociation, thus, 100.0%. As it can be seen, PB and CoFe-PBA have a slower iron dissociation, when compared to iron oxides and hydroxides, and present small values for free Fe²⁺ before 1 h. Besides, PB is completely dependent on UV-light exposure for a considerable amount of its dissociation, proving its low solubility. CoFe-PBA also depends on UV-light exposure; however, its structure bands are weaker, and a higher amount of iron is dissociated even without UV light. Iron oxide and (oxy)hydroxide were shown to be more soluble, presenting a higher amount of free iron even before 1 h. Although hematite still depends on UV-light exposure for a complete iron dissociation, for NiFeOOH and CoFe_x the UV-light effect on the dissociation is irrelevant. Hence, even if there are some differences in the dissociation behavior of the catalyst, also differences related to the [Fe(phen)₃]²⁺ complex formation for further spectroscopic iron quantification, the method was proven to be suitable for the quantification of iron in different thin films, with great and precise results.

Conclusions

The method proposed for iron quantification in thin films using 1,10-phenanthroline, preceded by a primary treatment using UV-light to ensure a full dissociation of

iron ions was shown to be highly effective, precise, and accurate. The analysis for different iron-based catalysts shows that the method has a wide range of applications in this area, being able to be applied for different structures. Besides, the method stands out as an easy and practical method, that can be performed in a fast way, at a low cost, and providing great results.

Supplementary Information

Supplementary data (precursors electronic spectra, UV-light reactor information, UV-light spectra, ICP-MS validation data and mechanism proposal) are available free of charge at <http://jbcbs.sbq.org.br> as PDF file.

Acknowledgments

All authors are grateful for the financial support of Brazilian Funding Agencies. This study was financed in part by the Coordenação de Aperfeiçoamento de Pessoal de Nível Superior - Brasil (CAPES) - Finance Code 001 and Process (88887.613265/2021-00), Conselho Nacional de Desenvolvimento Científico e Tecnológico CNPq (grant number 303231/2020-3 and 308203/2021-6) and Fundação de Amparo à Pesquisa do Estado de São Paulo, FAPESP (grant No. 2013/22127-2, 2014/50867-3, grant No. 2017/23960-0, grant No. 2017/11986-5, 2017/50085-3, grant No. 2018/25092-9, 2018/25207-0, 2019/00018-3, 2019/24445-8, 2019/00063-9, grant No. 2021/05976-2).

References

- Hunter, B. M.; Gray, H. B.; Müller, A. M.; *Chem. Rev.* **2016**, *116*, 14120. [Crossref]
- McCrorry, C. C. L.; Jung, S.; Peters, J. C.; Jaramillo, T. F.; *J. Am. Chem. Soc.* **2013**, *135*, 16977. [Crossref]
- Kozuch, S.; Martin, J. M. L.; *ACS Catal.* **2012**, *2*, 2787. [Crossref]
- Sallum, L. F.; Gonzalez, E. R.; Mota-Lima, A.; *Electrochem. Commun.* **2018**, *90*, 26. [Crossref]
- Li, D.; Liu, H.; Feng, L.; *Energy Fuels* **2020**, *34*, 13491. [Crossref]
- Hunter, B. M.; Thompson, N. B.; Müller, A. M.; Rossman, G. R.; Hill, M. G.; Winkler, J. R.; Gray, H. B.; *Joule* **2018**, *2*, 747. [Crossref]
- Kang, M.-S.; Choi, Y.-J.; Lee, H.-J.; Moon, S.-H.; *J. Colloid. Interface. Sci.* **2004**, *273*, 523. [Crossref]
- Du, P.; Eisenberg, R.; *Energy Environ. Sci.* **2012**, *5*, 6012. [Crossref]
- Villafranca, J. J.; Nowak, T. In *The Enzymes*, vol. 20; Sigman, D. S., ed.; Academic Press, 1992, p. 63-94. [Crossref]
- Li, J.; Huang, W.; Wang, M.; Xi, S.; Meng, J.; Zhao, K.; Jin, J.; Xu, W.; Wang, Z.; Liu, X.; Chen, Q.; Xu, L.; Liao, X.; Jiang, Y.; Owusu, K. A.; Jiang, B.; Chen, C.; Fan, D.; Zhou, L.; Mai, L.; *ACS Energy Lett.* **2019**, *4*, 285. [Crossref]
- Han, X.; He, G.; He, Y.; Zhang, J.; Zheng, X.; Li, L.; Zhong, C.; Hu, W.; Deng, Y.; Ma, T.-Y.; *Adv. Energy Mater.* **2018**, *8*, 1702222. [Crossref]
- Pires, B. M.; dos Santos, P. L.; Katic, V.; Strothauer, S.; Landers, R.; Formiga, A. L. B.; Bonacin, J. A.; *Dalton Trans.* **2019**, *48*, 4811. [Crossref]
- Amiais, R. S.; Donati, G. L.; Arruda, M. A. Z.; *TrAC, Trends Anal. Chem.* **2020**, *133*, 116094. [Crossref]
- Pessôa, G. S.; Lopes Jr., C. A.; Madrid, K. C.; Arruda, M. A. Z.; *Talanta* **2017**, *167*, 317. [Crossref]
- Agustina, E.; Goak, J.; Lee, S.; Seo, Y.; Park, J.-Y.; Lee, N.; *ChemistryOpen* **2015**, *4*, 613. [Crossref]
- Cai, H.; Liu, X.; Zou, J.; Xiao, J.; Yuan, B.; Li, F.; Cheng, Q.; *Chemosphere* **2018**, *193*, 833. [Crossref]
- Çağlar, Y.; Saka, E. T.; *Karbala Int. J. Mod. Sci.* **2017**, *3*, 185. [Crossref]
- Sabel, C. E.; Neureuther, J. M.; Siemann, S.; *Anal. Biochem.* **2009**, *397*, 218. [Crossref]
- Prenești, E.; Daniele, P. G.; Toso, S.; *Anal. Chim. Acta* **2002**, *459*, 323. [Crossref]
- Uddin, A. H.; Khalid, R. S.; Alaama, M.; Abdulkader, A. M.; Kasmuri, A.; Abbas, S. A.; *J. Anal. Sci. Technol.* **2016**, *7*, 6. [Crossref]
- Kuhn, D. D.; Young, T. C.; *Chemosphere* **2005**, *60*, 1222. [Crossref]
- Santos, C.; Alava-Moreno, F.; Lavilla, I.; Bendicho, C.; *J. Anal. At. Spectrom.* **2000**, *15*, 987. [Crossref]
- Druzian, G. T.; Pereira, L. S. F.; Mello, P. A.; Mesko, M. F.; Duarte, F. A.; Flores, E. M. M.; *J. Anal. At. Spectrom.* **2016**, *31*, 1185. [Crossref]
- Adamson, A. W.; *Coord. Chem. Rev.* **1993**, *125*, 1. [Crossref]
- Arellano, C. A. P.; Martínez, S. S.; *Sol. Energy Mater. Sol. Cells* **2010**, *94*, 327. [Crossref]
- Meeussen, J. C. L.; Keizer, M. G.; Van Riemsdijk, W. H.; De Haan, F. A. M.; *Environ. Sci. Technol.* **1992**, *26*, 1832. [Crossref]
- Machulek Jr., A.; Moraes, J. E. F.; Okano, L. T.; Silvério, C. A.; Quina, F. H.; *Photochem. Photobiol. Sci.* **2009**, *8*, 985. [Crossref]
- Subelzu, N.; Schöneich, C.; *Mol. Pharmaceutics* **2020**, *17*, 4163. [Crossref]
- Caicedo, D. F.; Brum, I. A. S.; Buitrago, L. A. B.; *REM, Int. Eng. J.* **2019**, *73*, 99. [Crossref]
- dos Santos, P. L.; Rowley-Neale, S. J.; Ferrari, A. G.-M.; Bonacin, J. A.; Banks, C.; *ChemElectroChem* **2019**, *6*, 5633. [Crossref]
- Braterman, P. S.; Song, J. I.; Peacock, R. D.; *Inorg. Chem.* **1992**, *31*, 555. [Crossref]

32. von Eschwege, K. G.; Conradie, J.; *Inorg. Chim. Acta* **2018**, *471*, 391. [Crossref]
33. Germscheidt, R. L.; Francischini, D. S.; Silva, M. B.; Arruda, M. A. Z.; Formiga, A. L. B.; da Rocha, T. C. R.; Bonacin, J. A.; *ACS Appl. Energy Mater.* **2022**, *5*, 9447. [Crossref]
34. Zhang, W.; Song, H.; Cheng, Y.; Liu, C.; Wang, C.; Khan, M. A. N.; Zhang, H.; Liu, J.; Yu, C.; Wang, L.; Li, J.; *Adv. Sci.* **2019**, *6*, 1801901. [Crossref]
35. Frenzel, N.; Hartley, J.; Frisch, G.; *Phys. Chem. Chem. Phys.* **2017**, *19*, 28841. [Crossref]
36. Ayers, J. B.; Waggoner, W. H.; *J. Inorg. Nucl. Chem.* **1971**, *33*, 721. [Crossref]
37. Alsaç, E. P.; Ülker, E.; Nune, S. V. K.; Dede, Y.; Karadas, F.; *Chem. Eur. J.* **2018**, *24*, 4856. [Crossref]
38. Zambiasi, P. J.; Aparecido, G. O.; Ferraz, T. V. B.; Skinner, W. S. J.; Yoshimura, R. G.; Moreira, D. E. B.; Germscheidt, R. L.; Nascimento, L. L.; Patrocinio, A. O. T.; Formiga, A. L. B.; Bonacin, J. A.; *Dalton Trans.* **2020**, *49*, 16488. [Crossref]
39. Al-Hakkani, M. F.; Gouda, G. A.; Hassan, S. H. A.; *Heliyon* **2021**, *7*, e05806. [Crossref]
40. Freitas, A. L. M.; Muche, D. N. F.; Leite, E. R.; Souza, F. L.; *J. Am. Ceram. Soc.* **2020**, *103*, 6833. [Crossref]
41. Lian, J.; Duan, X.; Ma, J.; Peng, P.; Kim, T.; Zheng, W.; *ACS Nano* **2009**, *3*, 3749. [Crossref]
42. Sherman, D. M.; Waite, T. D.; *Am. Min.* **1985**, *70*, 1262. [Crossref]
43. Goldsmith, Z. K.; Harshan, A. K.; Gerken, J. B.; Vörös, M.; Galli, G.; Stahl, S. S.; Hammes-Schiffer, S.; *PNAS* **2017**, *114*, 3050. [Crossref]
44. Santos, J. R. N.; Viégas, D. S. S.; Alves, I. C. B.; Rabelo, A. D.; Costa, W. M.; Marques, E. P.; Zhang, L.; Zhang, J.; Marques, A. L. B.; *Electrocatalysis* **2019**, *10*, 560. [Crossref]
45. Liardet, L.; Katz, J. E.; Luo, J.; Grätzel, M.; Hu, X.; *J. Mater. Chem. A* **2019**, *7*, 6012. [Crossref]

Submitted: September 7, 2022

Published online: January 10, 2023

